

1 **A new multi-variable benchmark for Last Glacial Maximum climate simulations**

2

3 Sean F. Cleator¹, Sandy P. Harrison², Nancy K. Nichols³, I. Colin Prentice⁴ and Ian
4 Roulstone¹

5

6 1: Department of Mathematics, University of Surrey, Guildford GU2 7XH, UK

7 2: School of Archaeology, Geography and Environmental Science, University of
8 Reading, Whiteknights, Reading, RG6 6AH, UK

9 3: Department of Mathematics & Statistics, University of Reading, Whiteknights,
10 Reading RG6 6AX, UK

11 4: AXA Chair of Biosphere and Climate Impacts, Department of Life Sciences,
12 Imperial College London, Silwood Park Campus, Buckhurst Road, Ascot SL5 7PY,
13 UK

14

15 Journal: *Climate of the Past*

16

17 **Abstract.** We present a new global reconstruction of seasonal climates at the Last
18 Glacial Maximum (LGM, 21,000 yr BP) made using 3-D variational data assimilation
19 with pollen-based site reconstructions of six climate variables and the ensemble average
20 of the PMIP3/CMIP5 simulations as a prior. We assume that the correlation matrix of
21 the uncertainties of the prior both spatially and temporally is Gaussian, in order to
22 produce a climate reconstruction that is smoothed both from month to month and from
23 grid cell to grid cell. The pollen-based reconstructions include mean annual temperature
24 (MAT), mean temperature of the coldest month (MTCO), mean temperature of the
25 warmest month (MTWA), growing season warmth as measured by growing degree
26 days above a baseline of 5°C (GDD₅), mean annual precipitation (MAP) and a moisture
27 index (MI), which is the ratio of MAP to mean annual potential evapotranspiration.
28 Different variables are reconstructed at different sites, but our approach both preserves
29 seasonal relationships and allows a more complete set of seasonal climate variables to
30 be derived at each location. We further account for the ecophysiological effects of low
31 atmospheric carbon dioxide concentration on vegetation in making reconstructions of
32 MAP and MI. This adjustment results in the reconstruction of wetter climates than
33 might otherwise be inferred by the vegetation composition. Finally, by comparing the
34 uncertainty contribution to the final reconstruction, we provide confidence intervals on
35 these reconstructions and delimit geographical regions for which the palaeodata provide
36 no information to constrain the climate reconstructions. The new reconstructions will
37 provide a benchmark created using clear and defined mathematical procedures that can
38 be used for evaluation of the PMIP4/CMIP6 entry-card LGM simulations and are
39 available at DOI:10.17864/1947.229.

40

41 **1 Introduction**

42 Models that perform equally well for present-day climate nevertheless produce very
43 different responses to anthropogenic forcing scenarios through the 21st century.
44 Although internal variability contributes to these differences, the largest source of
45 uncertainty in model projections in the first three to four decades of the 21st century
46 stems from differences in the response of individual models to the same forcing
47 (Kirtman et al., 2013). Thus, the evaluation of models based on modern observations is
48 not a good guide to their future performance, largely because the observations used to
49 assess model performance for present-day climate encompass too limited a range of
50 climate variability to provide a robust test of the ability to simulate climate changes.
51 Although past climate states do not provide analogues for the future, past climate
52 changes provide a unique opportunity for out-of-sample evaluation of climate model
53 performance (Harrison et al., 2015).

54
55 At the Last Glacial Maximum (LGM, conventionally defined for modelling
56 purposes as 21 000 years ago), insolation was quite similar to the present, but global
57 ice volume was at a maximum, eustatic sea level was close to a minimum, long-lived
58 greenhouse gas concentrations were lower, and atmospheric aerosol loadings higher
59 than today, and land surface characteristics (including vegetation distribution) were
60 also substantially different from today. These changes gave rise to a climate radically
61 different from that of today; indeed the magnitude of the change in radiative forcing
62 between LGM and pre-industrial climate is comparable to high-emissions projections
63 of climate change between now and the end of the 21st century (Braconnot et al., 2012).
64 The LGM has been a focus for model evaluation in the Paleoclimate Modelling
65 Intercomparison Project (PMIP) since its inception (Joussaume and Taylor, 1995;
66 Braconnot et al., 2007; Braconnot et al., 2012). The LGM is one of the two “entry card”
67 palaeoclimate simulations included in the current phase of the Coupled Model
68 Intercomparison Project (CMIP6) (Kageyama et al., 2018). The evaluation of previous
69 generations of palaeoclimate simulations has shown that the large-scale thermodynamic
70 responses seen in 21st century and LGM climates, including enhanced land–sea
71 temperature contrast, latitudinal amplification, and scaling of precipitation with
72 temperature, are likely to be realistic (Izumi et al., 2013; Li et al., 2013; Lunt et al,
73 2013; Hill et al., 2014; Izumi et al., 2014; Harrison et al., 2015). However, evaluation
74 against palaeodata shows that even when the sign of large-scale climate changes is
75 correctly predicted, the patterns of change at a regional scale are often inaccurate and
76 the magnitudes of change often underestimated (Brewer et al., 2007; Mauri et al., 2014;
77 Perez Sanz et al., 2014; Bartlein et al., 2017). The current focus on understanding what
78 causes mismatches between reconstructed and simulated climates is a primary
79 motivation for developing benchmark data sets that represent regional climate changes
80 comprehensively enough to allow a critical evaluation of model deficiencies.
81

82 Many sources of information can be used to reconstruct past climates. Pollen-based
83 reconstructions are the most widespread, and pollen-based data were the basis for the
84 current standard LGM benchmark data set by Bartlein et al. (2011). In common with
85 other data sources, the pollen-based reconstructions were generated for individual sites.
86 Geological preservation issues mean that the number of sites available inevitably
87 decreases through time (Bradley, 2014). Since pollen is only preserved for a long time
88 in anoxic sediments, the geographic distribution of potential sites is biased towards
89 climates that are relatively wet today. Furthermore, the actual sampling of potential
90 sites is highly non-uniform, so there are large geographic gaps in data coverage
91 (Harrison et al., 2016). The lack of continuous climate fields is not ideal for model
92 evaluation, and so attempts have been made to generalize the site-based data either
93 through gridding, interpolation, or some form of multiple regression (see e.g. Bartlein
94 et al., 2011; Annan and Hargreaves, 2013). However, there has so far been no attempt
95 to produce a physically consistent, multi-variable reconstruction which provides the
96 associated uncertainties explicitly.

97

98 A further characteristic of the LGM that creates problems for quantitative
99 reconstructions based on pollen data is the much lower atmospheric carbon dioxide
100 concentration, [CO₂], compared to the pre-industrial Holocene. [CO₂] has a direct effect
101 on plant physiological processes. Low [CO₂] as experienced by plants at the LGM is
102 expected to have led to reduced water-use efficiency – the ratio of carbon assimilation
103 to the water lost through transpiration (Bramley et al., 2013). Most reconstructions of
104 moisture variables from pollen data, including most of the reconstructions used by
105 Bartlein et al. (2011), do not take [CO₂] effects into account. Yet several modelling
106 studies have shown that the impact of low [CO₂] around the LGM on plant growth and
107 distribution was large (e.g. Jolly and Haxeltine, 1997; Cowling and Sykes, 1999;
108 Harrison and Prentice, 2003; Bragg et al., 2013; Martin Calvo et al., 2014; Martin Calvo
109 and Prentice, 2015). A few reconstructions of LGM climate based on the inversion of
110 process-based biogeography models have also shown large effects of low [CO₂] on
111 reconstructed LGM palaeoclimates (e.g. Guiot et al., 2000; Wu et al., 2007). The
112 reconstructions of moisture variables in the Bartlein et al. (2011) data set are thus
113 probably not reliable, and likely to be biased low.

114 Prentice et al. (2017) demonstrated an approach to correct reconstructions of moisture
115 variables for the effect of [CO₂], but this correction has not been applied globally. A
116 key side effect of applying this [CO₂] correction is to reconcile semi-quantitative
117 hydrological evidence for wet conditions at the LGM with the apparent dryness
118 suggested by the vegetation assemblages (Prentice et al., 2017). Similar considerations
119 apply to the interpretation of future climate changes in terms of vegetational effects.
120 Projections of future aridity (based on declining indices of moisture availability) linked
121 to warming are unrealistic, in a global perspective, because of the counteracting effect
122 of increased water use efficiency due to rising [CO₂] – which is generally taken into

123 account by process-based ecosystem models, but not by statistical models, using
124 projected changes in vapour pressure deficit or some measure of plant-available water
125 (Keenan et al., 2011; Roderick et al., 2015; Greve et al., 2017).

126

127 In this paper, we use variational data assimilation based on both pollen-based climate
128 reconstructions and climate model outputs to arrive at a best-estimate analytical
129 reconstruction of LGM climate, explicitly taking account of the impact of [CO₂].
130 Variational techniques provide a way of combining observations and model outputs to
131 produce climate reconstructions that are not exclusively constrained to one source of
132 information or the other (Nichols, 2010). We use the uncertainty contributions to the
133 analytical reconstruction to provide confidence intervals for these reconstructions and
134 also to delimit geographical regions for which the palaeodata provide no constraint on
135 the reconstructions. The resulting data set is expected provide a well-founded multi-
136 variable LGM climate dataset for palaeoclimate model benchmarking in CMIP6.

137

138

139 **2 Methods**

140 **2.1 Pollen-based climate reconstructions**

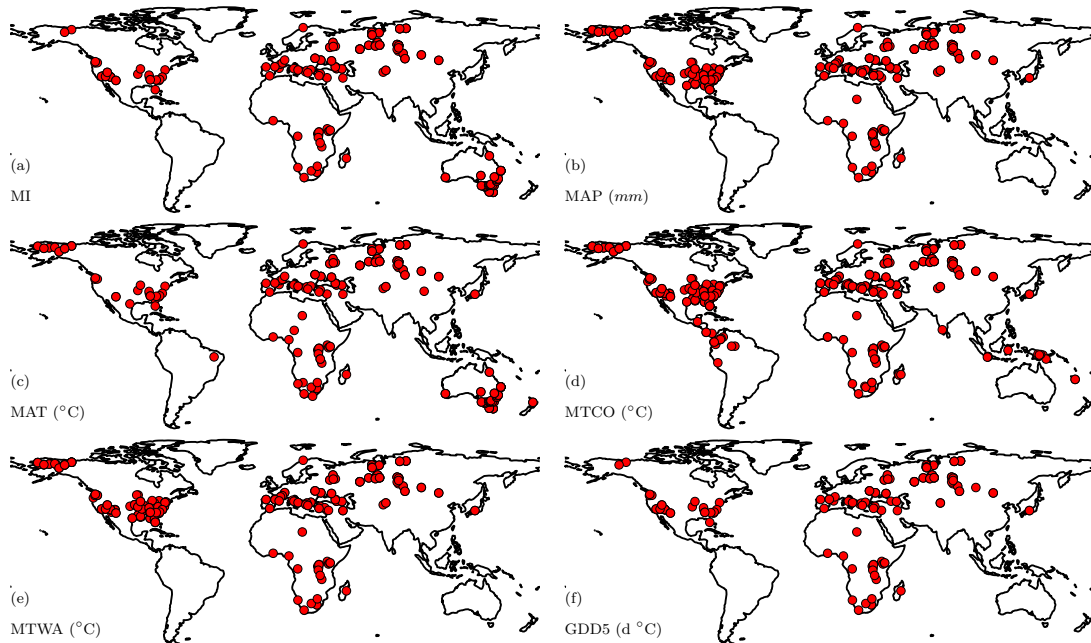
141

142 Bartlein et al. (2011) provided a global synthesis of pollen-based quantitative climate
143 reconstructions for the LGM. The Bartlein et al. (2011) data set includes reconstructions
144 of climate anomalies (differences between LGM and recent climates) for six variables
145 (and their uncertainties), specifically mean annual temperature (MAT), mean
146 temperature of the coldest month (MTCO), mean temperature of the warmest month
147 (MTWA), growing degree days above a baseline of above 5°C (GDD5), mean annual
148 precipitation (MAP), and an index of plant-available moisture (the ratio of actual to
149 equilibrium evapotranspiration, or α). There are a small number of LGM sites (94) in
150 the Bartlein et al. (2011) data set where model inversion was used to make the
151 reconstructions of α and MAP;. no [CO₂] correction is applied to these
152 reconstructions. There are no data from Australia in the Bartlein et al. (2011) data set,
153 and we therefore use quantitative reconstructions of MAT and another moisture index
154 (MI), the ratio of MAP to potential evapotranspiration, from Prentice et al. (2017).
155 Prentice et al. (2017) provide values of MI both before and after correction for [CO₂];
156 we use the uncorrected values in order to apply the correction for [CO₂] within our
157 assimilation framework. For consistency between the two data sets, we re-expressed
158 reconstructions of α in terms of MI via the Fu-Zhang formulation of the Budyko
159 relationship between actual evapotranspiration, potential evapotranspiration and
160 precipitation (Zhang et al., 2004; Gallego-Sala et al., 2016).

161

162 The spatial coverage of the final data set is uneven (Figure 1). There are many more
163 data points in Europe and North America than elsewhere. South America has the fewest

164 (14 sites). The number of variables available at each site varies: although most sites
165 (279) have reconstructions of at least three variables, some sites have reconstructions
166 of only one variable (60). Nevertheless, in regions where there is adequate coverage,
167 the reconstructed anomaly patterns are coherent, plausible and consistent among
168 variables.
169



170
171 Figure 1: The distribution of the site-based reconstructions of climatic variables at the
172 Last Glacial Maximum. The individual plots show sites providing reconstructions of
173 (a) moisture index (MI), (b) mean annual precipitation (MAP), (c) mean annual
174 temperature (MAT), (d) mean temperature of the coldest month (MTCO), (e) mean
175 temperature of the warmest month (MTWA) and growing degree days above a baseline
176 of 5° C (GDD5). The original reconstructions are from Bartlein et al. (2011) and
177 Prentice et al. (2017).

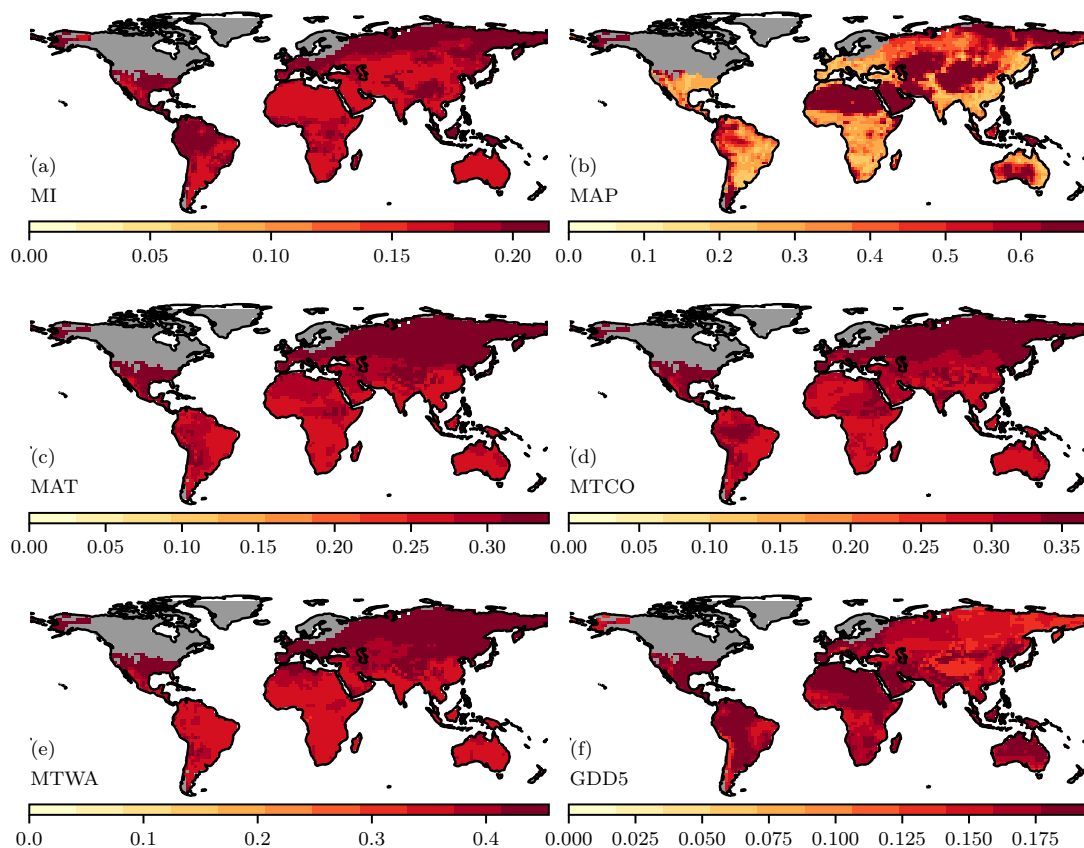
178
179 For this application, we derived absolute LGM climate reconstructions by adding the
180 reconstructed climate anomalies at each site to the modern climate values from the
181 Climate Research Unit (CRU) historical climatology data set (CRU CL v2.0 dataset,
182 New et al., 2002), which provides climatological averages of monthly temperature,
183 precipitation and cloud cover fraction for the period 1961-1990 CE. Most of the climate
184 variables (MTCO, MTWA, MAT, MAP) can be calculated directly from the CRU CL
185 v2.0 dataset. GDD5 was calculated from pseudo-daily data derived by linear
186 interpolation of the monthly temperatures. MI was calculated from the CRU climate
187 variables using the radiation calculations in the SPLASH model (Davis et al., 2017).
188 For numerical efficiency, we non-dimensionalised all of the absolute climate
189 reconstructions (and their standard errors) before applying the variational techniques
190 (for details, see Cleator et al., 2019a).

191

192

193 2.2 Climate model simulations

194 Eight LGM climate simulations (Table 1) from the third phase of the
195 Palaeoclimate Modelling Intercomparison Project (PMIP3: Braconnot et al., 2012)
196 were used to create a prior. The PMIP LGM simulations were forced by known changes
197 in incoming solar radiation, changes in land-sea geography and the extent and location
198 of ice sheets, and a reduction in $[\text{CO}_2]$ to 185 ppm (see Braconnot et al., 2012 for details
199 of the modelling protocol). We used the last 100 years of each LGM simulation. We
200 interpolated monthly precipitation, monthly temperature and monthly fraction of
201 sunshine hours from each LGM simulation and its pre-industrial (PI) control to a
202 common $2 \times 2^\circ$ grid. Simulated climate anomalies (LGM minus PI) for each grid cell
203 were then added to modern climate values calculated from the CRU CL 2.0 data set
204 (New et al., 2002), as described for the pollen-based reconstructions, to derive absolute
205 climate values. We calculated the multi-model mean and variance (Figure 2) across the
206 models for each of the climate variables to produce the gridded map used as the prior.
207



208

209 Figure 2: Uncertainties associated with the climate prior. The climate is derived from a
210 multi-model mean of the ensemble of models from the Palaeoclimate Modelling
211 Intercomparison Project (PMIP) and is shown in SI Figure 1. The uncertainties shown

212 here are the standard deviation of the multi-model ensemble values. The individual
213 plots show the variance for the simulated (a) moisture index (MI), (b) mean annual
214 precipitation (MAP), (c) mean annual temperature (MAT), (d) mean temperature of the
215 coldest month (MTCO), (e) mean temperature of the warmest month (MTWA) and
216 growing degree days above a baseline of 5° C (GDD5).

217

218 **2.3 Water-use efficiency calculations**

219

220 We applied the general approach developed by Prentice et al. (2017) to correct pollen-
221 based statistical reconstructions to account for [CO₂] effects. The approach as
222 implemented here is based on equations (Appendix 1) that link moisture index (MI) to
223 transpiration and the ratio of leaf-internal to ambient CO₂. The correction is based on
224 the principle that the rate of water loss per unit carbon gain is inversely related to
225 effective moisture availability as sensed by plants. The method involves solving a non-
226 linear equation that relates rate of water loss per unit carbon gain to MI, temperature
227 and CO₂ concentration. The equation is derived from theory that predicts the response
228 of the ratio of leaf-internal to ambient [CO₂] to vapour pressure deficit and temperature
229 (Prentice et al., 2014; Wang et al., 2014).

230

231 **2.4 Application of variational techniques**

232

233 Variational data assimilation techniques provide a way of combining observations
234 and model outputs to produce climate reconstructions that are not exclusively
235 constrained to one source of information or the other (Nichols, 2010). We use the
236 3D-variational method, described in Cleator et al. (2019a) to find the maximum a
237 posteriori estimate (or analytical reconstruction) of the palaeoclimate given the
238 site-based reconstructions and the model-based prior. The method constructs a
239 cost function, which describes how well a particular climate matches both the site-
240 based reconstructions and the prior, by assuming the reconstructions and prior
241 have a Gaussian distribution. To avoid sharp changes in time and/or space in the
242 analytical reconstructions, the method assumes that the prior temporal and
243 spatial covariance correlations are derived from a modified Bessel function, in
244 order to create a climate anomaly field that is smooth both from month to month
245 and from grid cell to grid cell. The degree of correlation is controlled through two
246 length scales: a spatial length scale that determines how correlated the covariance
247 in the prior is between different geographical areas, and a temporal length scale
248 that determines how correlated it is through the seasonal cycle. The site-based
249 reconstructions are assumed to have negligible correlations at these space and
250 time scales. The maximum a posteriori estimate is found by using the limited
251 memory Broyden- Fletcher-Goldfarb-Shanno method (Liu and Nocedal 1989) to

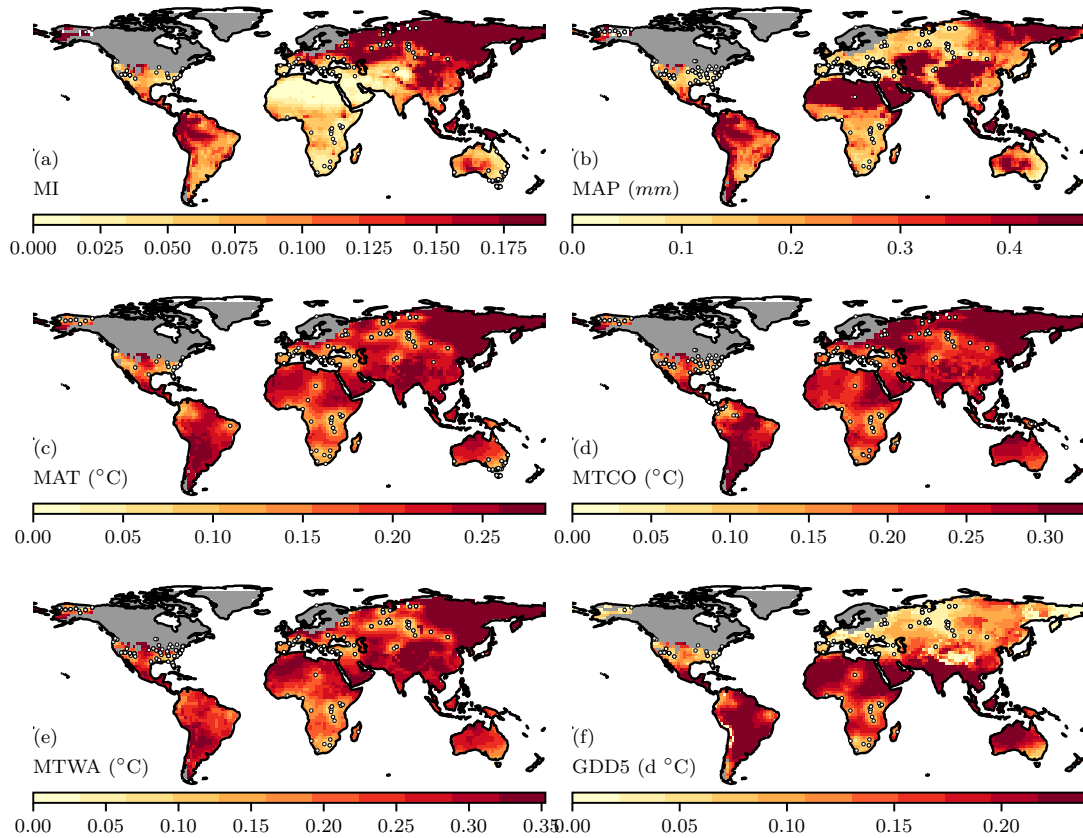
252 determine the climate that minimises the cost function. A first order estimate of
253 the analysis uncertainty covariance is also computed.

254

255 An observation operator based on calculations of the direct impact of [CO₂] on
256 water-use efficiency (section 2.3) is used in making the analytical reconstructions.
257 The prior is constructed as the average of eight LGM climate simulations (section
258 2.2). We use an ensemble of different model responses to the same forcing to
259 provide a series of physically consistent possible states, which can be viewed as
260 perturbed responses and provide the variance around the climatology provided
261 by the ensemble average. The prior uncertainty correlations are based on a
262 temporal length scale (Lt) of 1 month and a spatial length scale (Ls) of 400km.
263 Cleator et al., (2019a) have shown that a temporal length scale of 1 month
264 provides an adequately smooth solution for the seasonal cycle, both using single
265 sites and over multiple grid cells, as shown by the sensitivity of the resolution
266 matrix (Menke, 2012; Delahaies et al., 2017) to changes in the temporal length
267 scale. Consideration of the spatial spread of variance in the analytical
268 reconstruction shows that a spatial length scale of 400km also provides a
269 reasonable reflection of the large-scale coherence of regional climate change.

270

271 We generated composite variances on the analytical reconstructions (Figure 3) by
272 combining the covariances from the site-based reconstructions and from the
273 prior. There are regions where all of the models systematically differ from the site-
274 based reconstructions (Harrison et al., 2015) but nevertheless the inter-model
275 variability is low, which would lead to a very small contribution to the composite
276 uncertainties from the prior. We therefore calculated the uncertainty of the prior
277 from an equal combination of the global uncertainty, the average variance
278 between each grid cell, and local uncertainty, the variance between the different
279 models. The reliability of the analytical reconstructions was assessed by
280 comparing these composite covariances with the uncertainties in the prior. We
281 masked out cells where the inclusion of site-based reconstructions does not
282 produce an improvement of > 5% from the prior. Since this assessment is based
283 on a change in the variance, rather than absolute values, this masking removes
284 regions where there are no pollen-based reconstructions or the pollen-based
285 reconstructions have very large uncertainties.



286

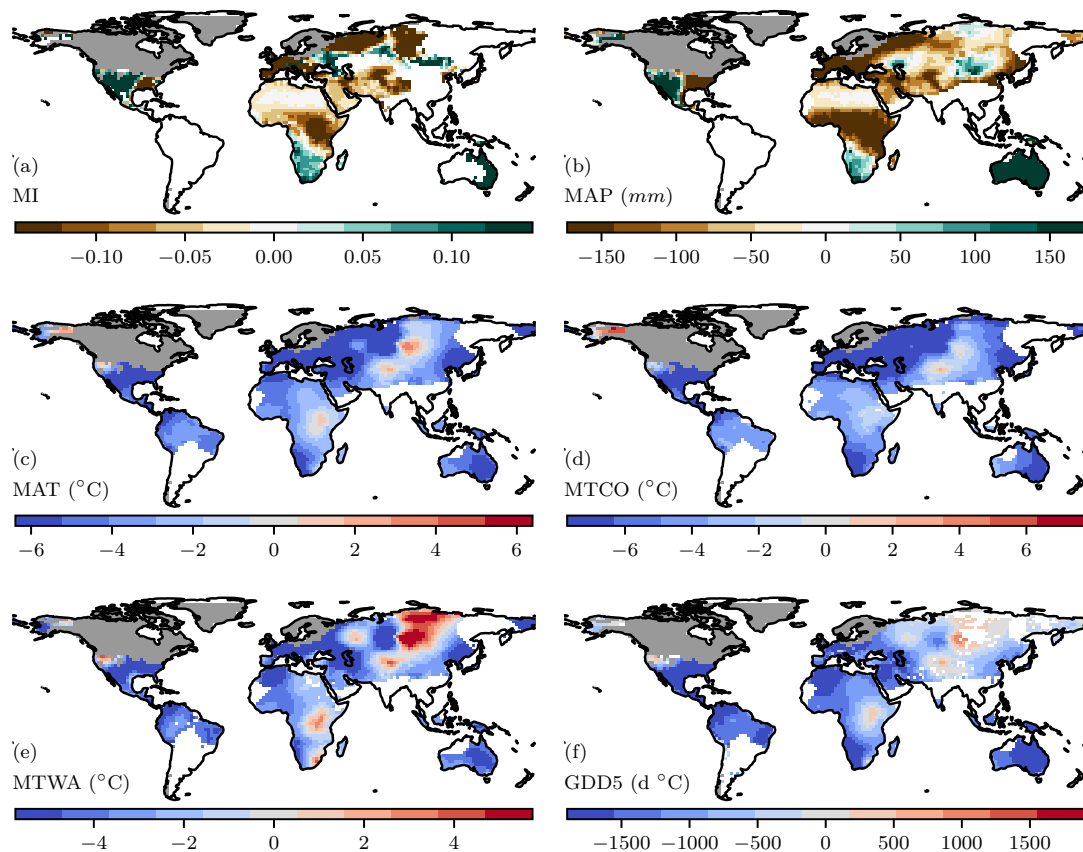
287 Figure 3: Uncertainties on the analytical reconstructions. These uncertainties represent
 288 a combination of the uncertainty on the site-based reconstructions, and the grid-based
 289 variance on the prior and the global variance from the prior.

290

291 3 Results

292

293 The analytical reconstructions (Figure 4) show an average year-round cooling of -5.6
 294 $^{\circ}\text{C}$ in the northern extratropics. The cooling is larger in winter (-7.6 $^{\circ}\text{C}$) than in summer
 295 (-2.4 $^{\circ}\text{C}$). A limited number of grid cells in central Eurasia show warmer-than-present
 296 summers, and higher MAT. Temperature changes are more muted in the tropics, with
 297 an average change in MAT of -3.7 $^{\circ}\text{C}$. The cooling is somewhat lower in summer than
 298 winter (-2.7 $^{\circ}\text{C}$ compared to -4.1 $^{\circ}\text{C}$). Reconstructed temperature changes were slightly
 299 larger in the southern extratropics, with average changes in MAT of -5.0 $^{\circ}\text{C}$, largely
 300 driven by cooling in winter.

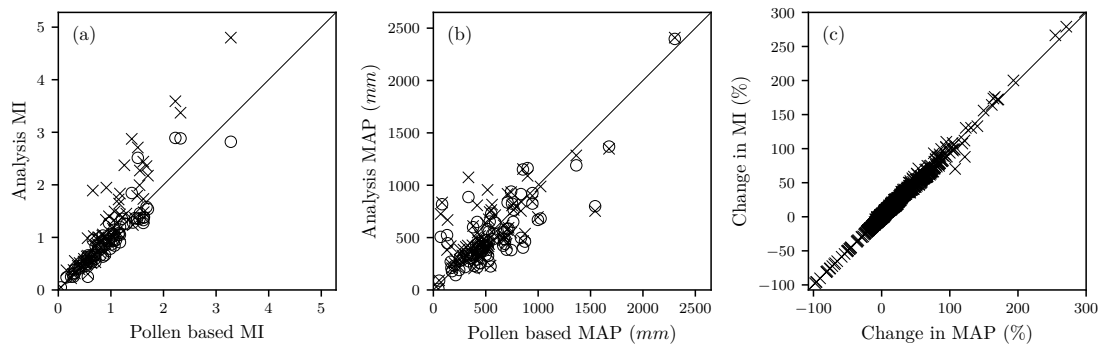


301
 302 Figure 4: Analytically reconstructed climate, where areas for which the site-based data
 303 provide no constraint on the prior have been masked out. The individual plots show
 304 reconstructed (a) moisture index (MI), (b) mean annual precipitation (MAP), (c) mean
 305 annual temperature (MAT), (d) mean temperature of the coldest month (MTCO), (e)
 306 mean temperature of the warmest month (MTWA) and growing degree days above a
 307 baseline of 5° C (GDD5). The anomalies are expressed relative to the long term average
 308 (1960-1990) values from the Climate Research Unit (CRU) historical climatology data
 309 set (CRU CL v2.0 dataset, New et al., 2002).

310
 311 Changes in moisture-related variables (MAP, MI) across the northern hemisphere are
 312 geographically more heterogeneous than temperature changes. Reconstructed MAP is
 313 greater than present in western North America (172 mm) but less than present (-29
 314 mm) in eastern North America. Most of Europe is reconstructed as drier than present
 315 (-305mm), the same for eastern Eurasia (-94 mm) and the Far East (-66 mm). The
 316 patterns in MI are not identical to those in MAP, because of the influence of temperature
 317 on MI, but regional changes are generally similar to those shown by MAP. Most of the
 318 tropics are shown as drier than present while the southern hemisphere extratropics are
 319 wetter than present, in terms of both MAP and MI.

320
 321 The reconstructed temperature patterns are not fundamentally different from those
 322 shown by Bartlein et al. (2011) but the analytical dataset provides information for a

323 much larger area (1153% increase) thanks to the method's imposition of consistency
 324 among different climate variables, and smooth variations both in space and through the
 325 seasonal cycle. There are systematic differences, however, between the analytical
 326 reconstructions and the pollen-based reconstructions in terms of moisture-related
 327 variables (MAP, MI) because the analytical reconstructions take account of the direct
 328 influence of $[CO_2]$ on plant growth. The physiological impact of $[CO_2]$ leads to
 329 analytical reconstructions indicating wetter than present conditions in many regions
 330 (Figure 5a, Figure 5b), for example in southern Africa where several of the original
 331 pollen-based reconstructions show no change in MAP or MI compared to present, but
 332 the analytical reconstruction shows wetter conditions than present. In some regions,
 333 incorporating the impact of $[CO_2]$ reverses the sign of the reconstructed changes. Part
 334 of northern Eurasia is reconstructed as being wetter than present, despite pollen-based
 335 reconstructions indicating conditions drier than present (both in terms of MAP and MI),
 336 as shown by SI Figure 3. The relative changes in MAP and MI are similar across all
 337 sites (Figure 5c), implying that the analytically reconstructed changes are driven by
 338 changes in precipitation rather than temperature.



339
 340 Figure 5: Impact of CO_2 on reconstructions of moisture-related variables. The
 341 individual plots show (a) the change in moisture index (MI) and (b) the change in mean
 342 annual precipitation (MAP) compared to the original pollen-based reconstructions for
 343 the LGM before (circles) and after (crosses) the physiological impacts of $[CO_2]$ on
 344 water-use efficiency are taken into account. The third plot (c) shows the relative
 345 difference in MI and MAP as a result of $[CO_2]$, shown as the percentage difference
 346 between the no- $[CO_2]$ and $[CO_2]$ calculations.

347

348 4 Discussion

349

350 Variational data assimilation techniques provide a way of combining observations and
 351 model outputs, taking account the uncertainties in both, to produce a best-estimate
 352 analytical reconstruction of LGM climate. These reconstructions extend the
 353 information available from site-based reconstructions both spatially and through the
 354 seasonal cycle. Our new analytical data set characterizes the seasonal cycle across a
 355 much larger region of the globe than the data set that is currently being used for
 356 benchmarking of palaeoclimate model simulations. We therefore suggest that this data

357 set (Cleator et al. 2019b) should be used for evaluating the CMIP6-PMIP4 LGM
358 simulations.

359

360 Some areas are still poorly covered by quantitative pollen-based reconstructions of
361 LGM climate, most notably South America. More pollen-based climate reconstructions
362 would provide one solution to this problem – and there are many pollen records that
363 could be used for this purpose (Flantua et al., 2015; Herbert and Harrison, 2016;
364 Harrison et al., 2016). There are also quantitative reconstructions of climate available
365 from individual sites (e.g. Lebamba et al., 2012; Wang et al., 2014; Loomis et al., 2017;
366 Camuera et al., 2019) that should be incorporated into future data syntheses. It would
367 also be possible to incorporate other sources of quantitative information, such as
368 chironomid-based reconstructions (e.g. Chang et al., 2015), within the variational data
369 assimilation framework.

370

371 One of the benefits of the analytical framework applied here is that it allows the
372 influence of changes in $[CO_2]$ on the moisture reconstructions to be taken into account.
373 Low $[CO_2]$ must have reduced plant water-use efficiency, because at low $[CO_2]$ plants
374 need to keep stomata open for longer in order to capture sufficient CO_2 . Statistical
375 reconstruction methods that use modern relationships between pollen assemblages and
376 climate under modern conditions (i.e. modern analogues, transfer functions, response
377 surfaces: see Bartlein et al., 2011 for discussion) cannot account for such effects.
378 Climate reconstruction methods based on the inversion of process-based ecosystem
379 models can do so (see e.g. Guiot et al., 2000; Wu et al., 2007; Wu et al., 2009; Izumi
380 and Bartlein, 2016) but are critically dependent on the reliability of the vegetation
381 model used. Most of the palaeoclimate reconstructions have been made by inverting
382 some version of the BIOME model (Kaplan et al., 2003), which makes use of
383 bioclimatic thresholds to separate different plant functional types (PFTs). As a result,
384 reconstructions made by inversion show “jumps” linked to shifts between vegetation
385 types dominated by different PFTs whereas, as has been shown recently (Wang et al.,
386 2017), differences in water use efficiency of different PFTs can be almost entirely
387 accounted for by a single equation, as proposed here. Sensitivity analyses show that the
388 numerical value of the corrected moisture variables (MI, MAP) is dependent on the
389 reconstructed values of these variables but is insensitive to uncertainties in the
390 temperature and moisture inputs (Prentice et al., 2017). The strength of the correction
391 is primarily sensitive to $[CO_2]$, but the LGM $[CO_2]$ value is well constrained from ice-
392 core records. The response of plants to changes in $[CO_2]$ is non-linear (Harrison and
393 Bartlein, 2012), and the effect of the change between recent and pre-industrial or mid-
394 Holocene conditions is less than that between pre-industrial and glacial conditions.
395 Nevertheless, it would be worth taking the $[CO_2]$ effect on water-use efficiency into
396 account in making reconstructions of interglacial time periods as well.

397

398 The influence of individual pollen-based reconstructions on the analytical
399 reconstruction of seasonal variability, or the geographic area influenced by an
400 individual site, is crucially dependent on the choice of length scales. We have adopted
401 conservative length scales of 1 month and 400 km, based on sensitivity experiments
402 made for southern Europe (Cleator et al., 2019a). These length scales produce
403 numerically stable results for the LGM, and the paucity of data for many regions at the
404 LGM means that using fixed, conservative length scales is likely to be the only practical
405 approach. However, in so far as the spatial length scale is related to atmospheric
406 circulation patterns, there is no reason to suppose that the optimal spatial length scale
407 will be the same from region to region. The density and clustering of pollen-based
408 reconstructions could also have a substantial effect on the optimal spatial length scale.
409 A fixed 1-month temporal length scale is appropriate for climates that have a reasonably
410 smooth and well-defined seasonal cycle, either in temperature or precipitation.
411 However, in climates where the seasonal cycle is less well defined, for example in the
412 wet tropics, or in situations where there is considerable variability on sub-monthly time
413 scales, other choices might be more appropriate. For time periods such as the mid-
414 Holocene, which have an order of magnitude more site-based data, it could be useful to
415 explore the possibilities of variable length scales.

416

417 We have used a 5% reduction in the analytical uncertainty compared to prior
418 uncertainty to identify regions where the incorporation of site-based data has a
419 negligible effect on the prior as a way of masking out regions for which the observations
420 have effectively no impact on the analytical reconstructions. The choice of a 5% cut-
421 off is arbitrary, but little would be gained by imposing a more stringent cut-off at the
422 LGM given that many regions are represented by few observations. A more stringent
423 cut-off could be applied for other time intervals with more data. We avoid the use of a
424 criterion based on the analytical reconstruction showing any improvement on the prior
425 because this could be affected by numerical noise in the computation. Alternative
426 criteria for the choice of cut-off could be based on whether the analytical reconstruction
427 had a reduced uncertainty compared to the pollen-based reconstructions or could be
428 derived by a consideration of the condition number used to select appropriate length
429 scales.

430

431 There have been a few previous attempts to use data assimilation techniques to generate
432 spatially continuous palaeoclimate reconstructions. Annan and Hargreaves (2013) used
433 a similar multi-model ensemble as the prior and the pollen-based reconstructions from
434 Bartlein et al. (2011) to reconstruct MAT at the LGM. However, they made no attempt
435 to reconstruct other seasonal variables, either independently, or through exploiting
436 features of the simulations (as we have done here) to generate seasonal reconstructions.
437 Particle filter approaches (e.g. Goosse et al., 2006; Dubinkina et al., 2011) produce
438 dynamic estimates of palaeoclimate, but particle filters cannot produce estimates of
439 climate outside the realm of the model simulations. Our 3-D variational data

440 assimilation approach has the great merit of being able to produce seasonally coherent
441 reconstructions generalized over space, while at the same time being capable of
442 producing reconstructions that are outside those captured by the climate model, because
443 they are not constrained by a specific source (Nichols, 2010). This property is of
444 particular importance if the resulting data set is to be used for climate model evaluation,
445 as we propose.

446
447 **Data availability.** The gridded data for the LGM reconstructions are available
448 from DOI:10.17864/1947.229; the code used to generate these reconstructions is
449 available from DOI:10.5281/zenodo.3445166.

450 **Author Contributions**

451 All authors contributed to the design of the study; ICP developed the theory
452 underlying the CO₂ correction; SC implemented the analyses. SC and SPH wrote
453 the first version of the manuscript, and all authors contributed to the final version.

454

455 **Competing Interests.**

456 The authors declare they have no competing interests.

457

458 **Acknowledgements**

459 SFC was supported by a UK Natural Environment Research Programme (NERC)
460 scholarship as part of the SCENARIO Doctoral Training Partnership. SPH
461 acknowledges support from the ERC-funded project GC 2.0 (Global Change 2.0:
462 Unlocking the past for a clearer future, grant number 694481). ICP acknowledges
463 support from the ERC under the European Union's Horizon 2020 research and
464 innovation programme (grant agreement no: 787203 REALM) This research is a
465 contribution to the AXA Chair Programme in Biosphere and Climate Impacts and the
466 Imperial College initiative on Grand Challenges in Ecosystems and the Environment
467 (ICP). NKN is supported in part by the NERC National Center for Earth Observation
468 (NCEO). We thank PMIP colleagues who contributed to the production of the
469 palaeoclimate reconstructions. We also acknowledge the World Climate Research
470 Programme's Working Group on Coupled Modelling, which is responsible for CMIP,
471 and the climate modelling groups in the Paleoclimate Modelling Intercomparison
472 Project (PMIP) for producing and making available their model output. For CMIP, the
473 U.S. Department of Energy's Program for Climate Model Diagnosis and
474 Intercomparison provides coordinating support and led development of software
475 infrastructure in partnership with the Global Organization for Earth System Science
476 Portals. The analyses and figures are based on data archived at CMIP on 12/09/18.

477

478 **References**

479 Annan, J.D., and Hargreaves, J.C.: A new global reconstruction of temperature changes
480 at the Last Glacial Maximum, *Clim. Past*, 9, 367-376,
481 <https://doi.org/10.5194/cp-9-367-2013>, 2013.

- 482 Bartlein, P.J., Harrison, S.P., Brewer, S., Connor, S., Davis, B.A.S., Gajewski, K.,
483 Guiot, J., Harrison-Prentice, T.I., Henderson, A., Peyron, O., Prentice, I.C.,
484 Scholze, M., Seppa, H., Shuman, B., Sugita, S., Thompson, R.S., Viau, A.E.,
485 Williams, J., and Wu, H.: Pollen-based continental climate reconstructions at 6
486 and 21 ka: a global synthesis, *Clim. Dynam.*, 37, 775-802,
487 <https://doi.org/10.1007/s00382-010-0904-1> 2011.
- 488 Bartlein, P.J., Harrison, S.P., and Izumi, K.: Underlying causes of Eurasian mid-
489 continental aridity in simulations of mid-Holocene climate, *Geophys. Res.*
490 *Letters*, 44, doi: 10.1002/2017GL074476, 2017.
- 491 Braconnot, P., Otto-Bliesner, B, Harrison, S.P., Joussaume, S., Peterschmitt, J-Y., Abe-
492 Ouchi, A., Crucifix, M., Driesschaert, E., Fichet, Th., Hewitt, C.D.,
493 Kageyama, M., Kitoh, A., Loutre, M-F., Marti, O., Merkel, U., Ramstein, G.,
494 Valdes, P., Weber, L., Yu, Y., and Zhao, Y.: Results of PMIP2 coupled
495 simulations of the mid-Holocene and Last Glacial Maximum, Part 1:
496 experiments and large-scale features, *Clim. Past*, 3, 261-277, doi:10.5194/cp-3-
497 261-2007, 2007.
- 498 Braconnot, P., Harrison, S.P., Kageyama, M., Bartlein, P.J., Masson-Delmotte, V.,
499 Abe-Ouchi, A., Otto-Bliesner, B., and Zhao, Y.: Evaluation of climate models
500 using palaeoclimatic data, *Nature Clim. Change*, 2, 417-424,
501 <https://doi.org/10.1038/nclimate1456>, 2012.
- 502 Bradley RS. 2014. *Paleoclimatology: Reconstructing Climates of the Quaternary*, 3rd
503 edn. Academic Press/Elsevier: Amsterdam.
- 504 Bragg, F., Prentice, I.C., Harrison, S.P., Foster, P.N., Eglinton, G., Rommerskirchen F.,
505 and Rullkötter, J.: n-Alkane stable isotope evidence for CO₂ as a driver of
506 vegetation change, *Biogeosci.*, 10, 2001–2010, [https://doi.org/10.5194/bg-10-](https://doi.org/10.5194/bg-10-2001-2013)
507 [2001-2013](https://doi.org/10.5194/bg-10-2001-2013), 2013.
- 508 Bramley, H., Turner, N., and Siddique, K.: Water use efficiency. In Kole, C.
509 (Ed.), *Genomics and Breeding for Climate-Resilient Crops* (1 ed., Vol. 2, pp.
510 487). Heidelberg: Springer. <https://doi.org/10.1007/978-3-642-37048-9>, 2013.
- 511 Brewer, S., Guiot, J., and Torre, F.: Mid-Holocene climate change in Europe: A data-
512 model comparison, *Clim. Past*, 3, 499–512, [https://doi.org/10.5194/cp-3-499-](https://doi.org/10.5194/cp-3-499-2007)
513 [2007](https://doi.org/10.5194/cp-3-499-2007), 2007.
- 514 Budich, R., Giorgetta, M., Jungclaus, J., Redler, R., and Reick, C.: The MPI-M
515 Millennium Earth System Model: An Assembling Guide for the COSMOS
516 Configuration.
517 [https://pure.mpg.de/rest/items/item_2193290_2/component/file_2193291/cont](https://pure.mpg.de/rest/items/item_2193290_2/component/file_2193291/content)
518 [ent](https://pure.mpg.de/rest/items/item_2193290_2/component/file_2193291/content), 2010 (last accessed 31/03/2019).
- 519 Camuera, J., Jimenez-Moreno, G., Ramos-Roman, M.J., Garcia-Alix, A., Toney, J.L.,
520 Anderson, R.S., Jimenez-Espejo, F., Bright, J., Webster, C., Yanes, Y., Carrion,
521 J.S.: Vegetation and climate changes during the last two glacial-interglacial
522 cycles in the western Mediterranean: A new long pollen record from Padul

523 (southern Iberian Peninsula). *Quat. Sci. Rev.*, 205, 86-105,
524 <https://doi.org/10.1016/j.quascirev.2018.12.013>, 2019.

525 Chang, J.C., Shulmeister, J., Woodward, C., Steinberger, L., Tibby, J., Barr, C.: A
526 chironomid-inferred summer temperature reconstruction from
527 subtropical Australia during the last glacial maximum (LGM) and the last
528 deglaciation. *Quat. Sci. Rev.*, 122, 282- 292,
529 <https://doi.org/10.1016/j.quascirev.2015.06.006>, 2015.

530 Cleator, S.F., Harrison, S.P., Nichols, N.K., Prentice, I.C., and Roustone, I.: A method
531 for generating coherent spatially explicit maps of seasonal palaeoclimates from
532 site-based reconstructions, arXiv:1902.04973 [math.NA], 2019a.

533 Cleator, S., Harrison, S. P., Nichols, N., Prentice, I. C., Roulstone, I.: A new multi-
534 variable benchmark for Last Glacial Maximum climate simulations. University
535 of Reading. Dataset. DOI:10.17864/1947.206, 2019b,

536 Cowling, S.A., and Sykes, M.T.: Physiological significance of low atmospheric CO₂
537 for plant-climate interactions, *Quatern. Res.*, 52, 237–242,
538 DOI: [10.1006/qres.1999.2065](https://doi.org/10.1006/qres.1999.2065), 1999.

539 Davis, T.W., Prentice, I.C., Stocker, B.D., Thomas, R.T., Whitley, R.J., Wang, H.,
540 Evans, B.J., Gallego-Sala, A.V., Sykes, M.T., and Cramer, W.: Simple process-
541 ed algorithms for simulating habitats (SPLASH v.1.0): robust indices of
542 radiation, evapotranspiration and plant-available moisture, *Geosci. Model*
543 *Develop.*, 10, 689-708, <https://doi.org/10.5194/gmd-10-689-2017>, 2017.

544 Delahaies, S., Roulstone, I., Nichols, N.: Constraining DALECv2 using multiple data
545 streams and ecological constraints: analysis and application. *Geosci. Model*
546 *Develop.*, 10, doi: 10.5194/gmd-10-2635- 2017, 2017.

547 Dubinkina, S., Goosse, H., Sallaz-Damaz, Y., Crespin, E., Crucifix, M.: Testing a
548 particle filter to reconstruct climate changes over the past centuries. *Int. J.*
549 *Bifurcation Chaos* 21, 3611-3618, 2011.

550 Dufresne, J.-L., Foujols, M.-A., Denvil, S., Caubel, A., Marti, O., Aumont, O.,
551 Balkanski, Y., Bekki, S., Bellenger, H., Benshila, R., Bony, S., Bopp, L.,
552 Braconnot, P., Brockmann, P., Cadule, P., Cheruy, F., Codron, F., Cozic, A.,
553 Cugnet, D., de Noblet, N., Duvel, J.-P., Ethé, C., Fairhead, L., Fichet, T.,
554 Flavoni, S., Friedlingstein, P., Grandpeix, J.-Y., Guez, L., Guilyardi, E.,
555 Hauglustaine, D., Hourdin, F., Idelkadi, A., Ghattas, J., Joussaume, S.,
556 Kageyama, M., Krinner, G., Labetoulle, S., Lahellec, A., Lefebvre, M.-P.,
557 Lefevre, F., Levy, C., Li, Z. X., Lloyd, J., Lott, F., Madec, G., Mancip, M.,
558 Marchand, M., Masson, S., Meurdesoif, Y., Mignot, J., Musat, I., Parouty, S.,
559 Polcher, J., Rio, C., Schulz, M., Swingedouw, D., Szopa, S., Talandier, C.,
560 Terray, P., Viovy, N., Vuichard, N.: Climate change projections using the IPSL-
561 CM5 Earth System Model: from CMIP3 to CMIP5, *Clim. Dyn.*, 40, 2123-2165,
562 DOI: 10.1007/s00382-012-1636-1, 2013.

563 Flantua, S.G.A., Hooghiemstra, H., Grimm, E.C., Behling, H., Bush, M.B., Gonzalez-
564 Arango, C., Gosling, W.D., Ledru, M.P., Lozano-Garcia, S., Maldonado, A.,

565 Prieto, A.R., Rull, V., and Van Boxel, J. H.: Updated site compilation of the
566 Latin American Pollen Database, *Rev. Palaeobot. Palyno.*, 223, 104–115,
567 <https://doi.org/10.1016/j.revpalbo.2015.09.008>, 2015.

568 Gallego-Sala, A., Charman, D., Li, G., Harrison, S.P., and Prentice, I.C.: Climate driven
569 expansion of blanket bogs in the British Isles during the Holocene, *Clim. Past*,
570 12, 129-136, <https://doi.org/10.5194/cp-12-129-2016>, 2016.

571 Gent, P.R., Danabasoglu, G., Donner, L.J., Holland, M.M., Hunke, E.C., Jayne, S.R.,
572 Lawrence, D.M., Neale, R.B., Rasch, P.J., Vertenstein, M., Worley, P.H., Yang,
573 Z-L., and Zhang, M.: The community climate system model version 4, *J. Clim.*,
574 24, 4973-4991, <https://doi.org/10.1175/2011JCLI4083.1>, 2011.

575 Goosse, H., Renssen, H., Timmermann, A., Bradley, R.S., and Mann, M.E.: Using
576 palaeoclimate proxy-data to select optimal realisations in an ensemble of
577 simulations of the climate of the past millennium, *Clim. Dynam.*, 27, 165-184,
578 DOI 10.1007/s00382-006-0128-6, 2006.

579 Greve, P., Roderick, M.L., and Seneviratne, S.I.: Simulated changes in aridity from the
580 last glacial maximum to 4xCO₂. *Environ. Res. Letters*, 12, 114021,
581 <https://iopscience.iop.org/article/10.1088/1748-9326/aa89a3/meta>, 2017.

582 Guiot, J., Torre, F., Jolly, D., Peyron, O., Boreux, J.J., and Cheddadi, R.: Inverse
583 vegetation modeling by Monte Carlo sampling to reconstruct palaeoclimates
584 under changed precipitation seasonality and CO₂ conditions: application to
585 glacial climate in Mediterranean region. *Ecological Modelling* 127: 119–140,
586 DOI: 10.1016/S0304-3800(99)00219-7, 2000.

587 Harrison, S.P., and Bartlein, P.J.: Records from the past, lessons for the future: what
588 the palaeo-record implies about mechanisms of global change, in: Henderson-
589 Sellers, A., and McGuffie, K. (Eds.), *The Future of the World's Climate*.
590 Elsevier, pp. 403-436, 2012.

591 Harrison, S.P., and Prentice, I.C.: Climate and CO₂ controls on global vegetation
592 distribution at the last glacial maximum: analysis based on palaeovegetation
593 data, biome modelling and palaeoclimate simulations, *Glob. Change Biol.*, 9,
594 983-1004, DOI: 10.1046/j.1365-2486.2003.00640.x, 2003.

595 Harrison, S.P., Bartlein, P.J., Brewer, S., Prentice, I.C., Boyd, M., Hessler, I.,
596 Holmgren, K., Izumi, K., and Willis, K.: Climate model benchmarking with
597 glacial and mid-Holocene climates, *Clim. Dynam.*, 43, 671-688, DOI:
598 10.1007/s00382-013-1922-6, 2014.

599 Harrison, S.P., Bartlein, P.J., Izumi, K., Li, G., Annan, J., Hargreaves, J., Braconnot,
600 P., and Kageyama, M.: Evaluation of CMIP5 palaeo-simulations to improve
601 climate projections, *Nature Clim. Change*, 5, 735-743,
602 <https://doi.org/10.1038/nclimate2649>, 2015.

603 Harrison, S.P., Bartlein, P.J., and Prentice, I.C.: What have we learnt from
604 palaeoclimate simulations?, *J. Quat. Sci.*, 31, 363-385, 2016.

605 Herbert, A.V., and Harrison, S.P.: Evaluation of a modern-analogue methodology for
606 reconstructing Australian palaeoclimate from pollen, *Rev. Palaeobot. Palynol.*,
607 226, 65-77, <https://doi.org/10.1016/j.revpalbo.2015.12.006>, 2016.

608 Hill, D.J., Haywood, A.M., Lunt, D.J., Hunter, S.J., Bragg, F.J., Contoux, C.,
609 Stepanek, C., Sohl, L., Rosenbloom, N.A., Chan, W-L., Kamae, Y., Zhang, Z.,
610 Abe-Ouchi, A., Chandler, M.A., Jost, A., Lohmann, G., Otto-Bliesner, B.L.,
611 Ramstein, G., and Ueda, H.: Evaluating the dominant components of warming
612 in Pliocene climate simulations, *Clim. Past*, 10, 79-90, DOI:10.5194/cp-10-79-
613 2014, 2014.

614 Izumi, K., and Bartlein, P.J.: North American paleoclimate reconstructions for the Last
615 Glacial Maximum using an inverse modeling through iterative forward
616 modeling approach applied to pollen data, *Geophys. Res. Letters*, 43,
617 doi:10.1002/2016GL070152, 2016.

618 Izumi, K., Bartlein, P.J., and Harrison, S.P.: Consistent behaviour of the climate system
619 in response to past and future forcing, *Geophys. Res. Letters*, 40, 1817-1823,
620 DOI:10.1002/grl.50350, 2013.

621 Izumi, K., Bartlein, P.J., and Harrison, S.P.: Energy-balance mechanisms underlying
622 consistent large-scale temperature responses in warm and cold climates, *Clim.*
623 *Dynam.*, 44, 3111-3127, DOI: 10.1007/s00382-014-2189-2, 2014.

624 Jolly, D., and Haxeltine, A.: Effect of low glacial atmospheric CO₂ on tropical African
625 montane vegetation, *Science*, 276, 786-788, DOI:
626 10.1126/science.276.5313.786, 1997.

627 Joussaume, S. and Taylor, K. E.: Status of the Paleoclimate Modeling Intercomparison
628 Project (PMIP), In: *Proceedings of the First International AMIP Scientific*
629 *Conference*, WCRP Report, 425-430, 1995.

630 Jungclaus, J.H., Keenlyside, N., Botzet, M., Haak, H., Luo, J-J., Latif, M., Marotzke,
631 J., Mikolajewicz, U., and Roeckner, E.: Ocean circulation and tropical
632 variability in the coupled model ECHAM5/MPI-OM, *J. Clim.*, 19, 3952-3972,
633 DOI: 10.1175/JCLI3827.1, 2006.

634 Kageyama, M., Braconnot, P., Harrison, S.P., Haywood, A.M., Jungclaus, J.H., Otto-
635 Bliesner, B.L., Peterschmitt, J.Y., Abe-Ouchi, A., Albani, S., Bartlein, P.J.,
636 Brierley, C., Crucifix, M., Dolan, A., Fernandez-Donado, L., Fischer, H.,
637 Hopcroft, P.O., Ivanovic, R.F., Lambert, F., Lunt, D.J., Mahowald, N.M.,
638 Peltier, W.R., Phipps, S.J., Roche, D.M., Schmidt, G.A., Tarasov, L., Valdes,
639 P.J., Zhang, Q., and Zhou, T.: The PMIP4 contribution to CMIP6: Part 1:
640 Overview and over-arching analysis plan, *Geosci. Model Develop.*, 11, 1033-
641 1057, <https://doi.org/10.5194/gmd-11-1033-2018>, 2018.

642 Kaplan, J.O., Bigelow, N.H., Bartlein, P.J., Christensen, T.R., Cramer, W., Harrison,
643 S.P., Matveyeva, N.V., McGuire, A.D., Murray, D.F., Prentice, I.C., Razzhivin,
644 V.Y., Smith, B. and Walker, D.A., Anderson, P.M., Andreev, A.A., Brubaker,
645 L.B., Edwards, M.E., and Lozhkin, A.V.: Climate change and Arctic
646 ecosystems II: Modeling, palaeodata-model comparisons, and future

647 projections, *J. Geophys. Res.-Atmosphere* 108, No. D19, 8171, DOI:
648 10.1029/2002JD002559, 2003.

649 Keenan, T., Serra, J.M., Lloret, F., Ninyerola, M., and Sabate, S.: Predicting the future
650 of forests in the Mediterranean under climate change, with niche- and process-
651 based models: CO₂ matters! *Glob. Change Biol.*, 17, 565-579, DOI:
652 10.1111/j.1365-2486.2010.02254.x, 2011.

653 Kirtman, B., Power, S.B., Adedoyin, J.A., Boer, G.J., Bojariu, R., Camilloni, I., Doblas-
654 Reyes, F.J., Fiore, A.M., Kimoto, M., Meehl, G.A., Prather, M., Sarr, A., Schär,
655 C., Sutton, R., van Oldenborgh, G.J., Vecchi G., and Wang, H.J.: Near-term
656 climate change: projections and predictability. In *Climate Change 2013: the*
657 *Physical Science Basis. Contribution of Working Group I to the Fifth*
658 *Assessment Report of the Intergovernmental Panel on Climate Change*, Stocker
659 TF, Qin D, Plattner G-K, Tignor M, Allen SK, Boschung J, Nauels A, Xia Y,
660 Bex V, Midgley PM (eds). Cambridge University Press, Cambridge, UK, 953–
661 1028, 2013.

662 Lebamba, J., Vincens, A., Maley, J.: Pollen, vegetation change and climate at Lake
663 Barombi Mbo (Cameroon) during the last ca. 33 000 cal yr BP: a numerical
664 approach. *Clim. Past*, 8, 59-78, <https://doi.org/10.5194/cp-8-59-2012>,
665 2012.

666 Li, G., Harrison, S.P., Bartlein, P.J., Izumi, K., and Prentice, I.C.: Precipitation scaling
667 with temperature in warm and cold climates: an analysis of CMIP5 simulations,
668 *Geophys. Res. Letters*, 40, 4018-4024, doi:10.1002/grl.50730, 2013.

669 Li, L., Lin, P., Yu, Y., Wang, B., Zhou, T., Liu, L., Liu, J., Bao, Q., Xu, S., Huang, W.,
670 Xia, K., Pu, Y., Dong, L., Shen, S., Liu, Y., Hu, N., Liu, M., Sun, W., Shi, X.,
671 Zheng, W., Wu, B., Song, M., Liu, H., Zhang, X., Wu, G., Xue, W., Huang, X.,
672 Yang, G., Song, Z., and Qiao, F.: The flexible global ocean-atmosphere-land
673 system model, Grid-point Version 2: FGOALS-g2. *Advan. Atmos. Sci.*, 30,
674 543-560, <https://doi.org/10.1007/s00376-012-2140-6>, 2013.

675 Liu, D. C., Nocedal, J.: On the limited memory BFGS method for large scale
676 optimization. *Math. Programming*, 45, 503–528, doi:
677 10.1007/BF01589116, 1989.

678 Loomis, S. E., Russell, J. M., Verschuren, D., Morrill, C., De Cort, G., Sinninghe
679 Damste, J. S., Olago, D., Eggermont, H., Street-Perrott, F.A., Kelly, M. A.: The
680 tropical lapse rate steepened during the Last Glacial Maximum. *Science*
681 *Advances*, 3, e1600815.doi:10.1126/sciadv.1600815, 2017.

682 Lunt, D.J., Abe-Ouchi, A., Bakker, P., Berger, A., Braconnot, P., Charbit, S., Fischer,
683 N., Herold, N., Jungclaus, J. H., Khon, V. C., Krebs-Kanzow, U., Langebroek,
684 P. M., Lohmann, G., Nisancioglu, K. H., Otto-Bliesner, B. L., Park, W., Pfeiffer,
685 M., Phipps, S. J., Prange, M., Rachmayani, R., Renssen, H., Rosenbloom, N.,
686 Schneider, B., Stone, E. J., Takahashi, K., Wei, W., Yin, Q., and Zhang, Z. S.:
687 A multi-model assessment of last interglacial temperatures. *Clim. Past*, 9, 699–
688 717, DOI: 10.5194/cp-9-699-2013, 2013.

689 Martin Calvo, M., Prentice, I.C., and Harrison, S.P.: Climate versus carbon dioxide
690 controls on biomass burning: a model analysis of the glacial-interglacial
691 contrast, *Biogeosci.*, 11, 6017–6027, DOI:10.5194/bg-11-6017-2014, 2014.

692 Martin Calvo, M., and Prentice, I.C.: Effects of fire and CO₂ on biogeography and
693 primary production in glacial and modern climates, *N. Phytol.*, 208, 987–
694 994, <https://doi.org/10.1111/nph.13485>, 2015.

695 Mauri, A., Davis, B.A.S., Collins, P.M., and Kaplan, J.O.: The influence of atmospheric
696 circulation on the mid-Holocene climate of Europe: a data-model comparison.
697 *Climate of the Past* 10: 1925–1938, DOI: 10.5194/cp-10-1925-2014, 2014.

698 Menke, W.: *Geophysical data analysis: Discrete inverse theory (Matlab 3rd ed.)*.
699 Cambridge, Massachusetts: Academic Press, 2012.

700 New, M., Lister, D., Hulme, M., and Makin, I.: A high-resolution data set for surface
701 climate over global land areas, *Clim. Res.*, 21, 1-25, 2002.

702 Nichols, N.K.: *Mathematical concepts of data assimilation*, In: Lahoz, W., Khatatov,
703 B., and Menard, R. (Eds.), *Data Assimilation*, Springer, 2010.

704 Perez-Sanz, A., Li, G., Gonzalez, P., and Harrison, S.P.: Evaluation of seasonal
705 climates of northern Africa and the Mediterranean in the CMIP5 simulations,
706 *Clim. Past*, 10, 551-568, DOI:10.5194/cp-10-551-2014, 2014.

707 Prentice, I.C., Dong, N., Gleason, S.M., Maire, V., and Wright, I.J.: Balancing the costs
708 of carbon gain and water loss: testing a new quantitative framework for plant
709 functional ecology, *Ecol. Letters*, 17, 82-91, <https://doi.org/10.1111/ele.12211>,
710 2014.

711 Prentice, I.C., Cleator, S.F., Huang, Y.H., Harrison, S.P., and Roulstone, I.:
712 Reconstructing ice-age palaeoclimates: Quantifying low-CO₂ effects on plants,
713 *Glob. Planet. Change*, 149, 166-176,
714 <https://doi.org/10.1016/j.gloplacha.2016.12.012>, 2017.

715 Schmidt, G.A., Ruedy, R., Hansen, J.E., Aleinov, I., Bell, N., Bauer, M., Bauer, S.,
716 Cairns, B., Canuto, V., Cheng, Y., Del Genio, A., Faluvegi, G., Friend, A.D.,
717 Hall, T.M., Hu, Y., Kelley, M., Kiang, N.Y., Koch, D., Lacis, A.A., Lerner, J.,
718 Lo, K.K., Miller, R.L., Nazarenko, L., Oinas, V., Perlwitz, J., Perlwitz, J., Rind,
719 D., Romanou, A., Russell, G.L., Sato, M., Shindell, D.T., Stone, P.H., Sun, S.,
720 Tausnev, N., Thresher, D., and Yao, M-S.: Present day atmospheric simulations
721 using GISS ModelE: Comparison to in situ, satellite and reanalysis data, *J.*
722 *Clim.*, 19, 153-192, <https://doi.org/10.1175/JCLI3612.1>, 2006.

723 Roderick, M.L., Greve, P., and Farquhar, G.D.: On the assessment of aridity with
724 changes in atmospheric CO₂, *Water Resour. Res.*, 51, 5450–63,
725 DOI:10.1002/2015WR017031, 2015.

726 Voldoire, A., Sanchez-Gomez, E., Salas y Mélia, D., Decharme, B., Cassou, C., Sénési,
727 S., Valcke, S., Beau, I., Alias, A., Chevallier, M., Déqué, M., Deshayes, J.,
728 Douville, H., Fernandez, E., Madec, G., Maisonnave, E., Moine, M-P., Planton,
729 M.S., Saint-Martin, D., Szopa, S., Tyteca, S., Alkama, R., Belamari, S., Braun,
730 A., Coquart, L., and Chauvin, F.: The CNRM-CM5.1 global climate model:

731 description and basic evaluation, *Clim Dyn.*, 759, doi:10.1007/s00382-011-
732 1259-y, 2012.

733 Wang, H., Prentice, I.C., and Davis, T.W.: Biophysical constraints on gross primary
734 production by the terrestrial biosphere, *Biogeosci.*, 11, 5987-6001,
735 <https://doi.org/10.5194/bg-11-5987-2014>, 2014.

736 Wang, H., Prentice, I.C., Cornwell, W.M, Keenan, T.F., Davis, T.W., Wright, I.J.,
737 Evans, B.J., and Peng, C.: Towards a universal model for carbon dioxide uptake
738 by plants, *Nature Plants*, 3, 734–741, [https://doi.org/10.1038/s41477-017-
739 0006-8](https://doi.org/10.1038/s41477-017-0006-8), 2017.

740 Wang, Y., Herzsuh, U., Shumilovskikh, L. S., Mischke, S., Birks, H. J. B.,
741 Wischniewski, J., Bohner, J., Schlutz, F., Lehmkuhl, F., Diekmann, B.,
742 Wunnemann, B., Zhang, C.: Quantitative reconstruction of precipitation
743 changes on the NE Tibetan Plateau since the Last Glacial Maximum –
744 extending the concept of pollen source area to pollen-based climate
745 reconstructions from large lakes, *Clim. Past*, 10, 21-39,
746 <https://doi.org/10.5194/cp-10-21-2014>, 2014.

747 Watanabe, S., Hajima, T., Sudo, K., Nagashima, T., Takemura, T., Okajima, H.,
748 Nozawa, T., Kawase, H., Abe, M., Yokohata, T., Ise, T., Sato, H., Kato, E.,
749 Takata, K., Emori., S., Kawamiya, M.: MIROC-ESM: model description and
750 basic results of CMIP5-20c3m experiments, *Geosci. Mod. Dev.*, 4, 845-872,
751 <https://doi.org/10.5194/gmd-4-845-2011>, 2011.

752 Wu, H., Guiot, J., Brewer, S., Guo, Z.: Climatic changes in Eurasia and Africa at the
753 Last Glacial Maximum and mid-Holocene: reconstruction from pollen data
754 using inverse vegetation modelling, *Clim. Dynam.*, 29, 211–229, DOI:
755 10.1007/s00382-007-0231-3, 2007.

756 Wu, H., T. Guiot, J., Peng, C., and Guo, Z.: New coupled model used inversely for
757 reconstructing past terrestrial carbon storage from pollen data: Validation of
758 model using modern data, *Glob. Change Biol.*, 15, 82–96,
759 <https://doi.org/10.1111/j.1365-2486.2008.01712.x>, 2009.

760 Yukimoto, S., Yoshimura, H., Hosaka, M., Sakami, T., Tsujino, H., Hirabara, M.,
761 Tanaka, T.Y., Deushi, M., Obata, A., Nakano, H., Adachi, Y., Shindo, E., Yabu,
762 S., Ose, T., Kitoh, A.: Meteorological Research Institute-Earth System Model
763 v1 (MRI-ESM1) – Model Description, *Tech. Rep. Meteor. Res. Inst.*, 64, 88 pp.,
764 http://www.mri-jma.go.jp/Publish/Technical/DATA/VOL_64/index.html,
765 2011.

766 Zhang, L., Hickel, K., Dawes, W.R., Chiew, F.H.S., Western, A.W., Briggs, P.R.: A
767 rational function approach for estimating mean annual evapotranspiration.
768 *Water Resources Research* 40, W02502, DOI:10.1029/2003WR002710, 2004.
769
770
771

772 **Figures and Tables Captions**

773

774 Figure 1: The distribution of the site-based reconstructions of climatic variables at the
775 Last Glacial Maximum. The individual plots show sites providing reconstructions of
776 (a) moisture index (MI), (b) mean annual precipitation (MAP), (c) mean annual
777 temperature (MAT), (d) mean temperature of the coldest month (MTCO), (e) mean
778 temperature of the warmest month (MTWA) and growing degree days above a baseline
779 of 5° C (GDD5). The original reconstructions are from Bartlein et al. (2011) and
780 Prentice et al. (2017).

781

782 Figure 2: Uncertainties associated with the climate prior. The climate is derived from a
783 multi-model mean of the ensemble of models from the Palaeoclimate Modelling
784 Intercomparison Project (PMIP) and is shown in SI Figure 1. The uncertainties shown
785 here are the standard deviation of the multi-model ensemble values. The individual
786 plots show the variance for the simulated (a) moisture index (MI), (b) mean annual
787 precipitation (MAP), (c) mean annual temperature (MAT), (d) mean temperature of the
788 coldest month (MTCO), (e) mean temperature of the warmest month (MTWA) and
789 growing degree days above a baseline of 5° C (GDD5).

790

791 Figure 3: Uncertainties on the analytical reconstructions. These uncertainties
792 represent a combination of the uncertainty on the site-based reconstructions, and
793 the grid-based variance on the prior and the global variance from the prior.

794

795 Figure 4: Analytically reconstructed climate, where areas for which the site-based data
796 provide no constraint on the prior have been masked out. The individual plots show
797 reconstructed (a) moisture index (MI), (b) mean annual precipitation (MAP), (c) mean
798 annual temperature (MAT), (d) mean temperature of the coldest month (MTCO), (e)
799 mean temperature of the warmest month (MTWA) and growing degree days above a
800 baseline of 5° C (GDD5). The anomalies are expressed relative to the long term average
801 (1960-1990) values from the Climate Research Unit (CRU) historical climatology data
802 set (CRU CL v2.0 dataset, New et al., 2002).

803

804

805 Figure 5: Impact of CO₂ on reconstructions of moisture-related variables. The
806 individual plots show (a) the change in moisture index (MI) and (b) the change in mean
807 annual precipitation (MAP) compared to the original pollen-based reconstructions for
808 the LGM before (circles) and after (crosses) the physiological impacts of [CO₂] on
809 water-use efficiency are taken into account. The third plot (c) shows the relative
810 difference in MI and MAP as a result of [CO₂], shown as the percentage difference
811 between the no-[CO₂] and [CO₂] calculations.

812

813 Table 1: Details of the models from the Palaeoclimate Modelling Intercomparison
 814 Project (PMIP) that were used for the Last Glacial Maximum (LGM) simulations used
 815 to create the prior.

816

817 Table 1: *Details of the models from the third phase of the Palaeoclimate Modelling*
 818 *Intercomparison Project (PMIP3) that were used for the Last Glacial Maximum*
 819 *(LGM) simulations used to create the prior. Coupled ocean-atmosphere models are*
 820 *indicated as OA, which OAC models have a fully interactive carbon cycle. The*
 821 *resolution in the atmospheric, oceanic and sea ice components of the models is given*
 822 *in terms of numbers of grid cells in latitude and longitude.*

823

Model name	Type	Resolution			Year length	Reference
		Atmosphere	Ocean	Sea Ice		
CCSM4	OA	192, 288	320, 384	320, 384	365	Gent et al. (2011)
CNRM-CM5	OA	128, 256	292, 362	292, 362	365-366	Voltaire et al. (2012)
MPI-ESM-P	OA	96, 192	220, 256	220, 256	365-366	Jungclaus et al. (2006)
MRI-CGCM3	OA	160, 320	360, 368	360, 368	365	Yukimoto et al. (2011)
FGOALS-g2	OA	64, 128	64, 128	64, 128	365	Li et al. (2013)
COSMOS-ASO	OAC	96, 48	120, 101	120, 101	360	Budich et al. (2010)
IPSL-CM5A-LR	OAC	96, 96	149, 182	149, 182	365	Dufresne et al., 2013
MIROC-ESM	OAC	64, 128	192, 256	192, 256	365	Watanabe et al. (2011)

824

825 Appendix

826 We define e as the water lost by transpiration (E) per unit carbon gained by
827 photosynthesis (A). This term, the inverse of the water use efficiency, is given by:

$$828 \quad e = E/A = 1.6 D / ((1 - \chi) c_a) \quad (\text{A1})$$

829 where D is the leaf-to-air vapour pressure deficit (Pa), c_a is the ambient CO₂ partial
830 pressure (Pa) and χ is the ratio of leaf-internal CO₂ partial pressure (c_i) to c_a . An
831 optimality-based model (Prentice *et al.* 2014), which accurately reproduces global
832 patterns of χ and its environmental dependencies inferred from leaf $\delta^{13}\text{C}$ measurements
833 (Wang *et al.* 2017), predicts that:

$$834 \quad \chi = (\Gamma^*/c_a) + (1 - \Gamma^*/c_a) \xi / (\xi + \sqrt{D}) \quad (\text{A2a})$$

835 and

$$836 \quad \xi = \sqrt{(\beta(K + \Gamma^*)/1.6 \eta^*)} \quad (\text{A2b})$$

837 where Γ^* is the photorespiratory compensation point of C₃ photosynthesis (Pa), β is a
838 constant (estimated as 240 by Wang *et al.* 2017), K is the effective Michaelis-Menten
839 coefficient of Rubisco (Pa), and η^* is the ratio of the viscosity of water (Pa s) at ambient
840 temperature to its value at 25°C. Here K depends on the Michaelis-Menten coefficients
841 of Rubisco for carboxylation (K_C) and oxygenation (K_O), and on the partial pressure of
842 oxygen O (Farquhar *et al.* 1980):

$$843 \quad K = K_C (1 + O/K_O) \quad (\text{A3})$$

844 Standard values and temperature dependencies of K_C , K_O , Γ^* and η^* are assigned as in
845 Wang *et al.* (2017).

846 The moisture index MI is expressed as

$$847 \quad \text{MI} = P/E_q, \quad E_q = \sum_n (R_n/\lambda) s / (s + \gamma) \quad (\text{A4})$$

848 where P is annual precipitation, R_n is net radiation for month n , λ is the latent heat of
849 vaporization of water, s is the derivative of the saturated vapour pressure of water with
850 respect to temperature (obtained from a standard empirical formula also used by Wang
851 *et al.* 2017), and γ is the psychrometer constant. We assume that values of MI
852 reconstructed from fossil pollen assemblages, using contemporary pollen and climate
853 data either in a statistical calibration method or in a modern-analogue search, need to
854 be corrected in such a way as to preserve the contemporary relationship between MI
855 and e , while taking into account the change in e that is caused by varying c_a and
856 temperature away from contemporary values. The sequence of calculations is as
857 follows. (1) Estimate e and its derivative with respect to temperature ($\partial e/\partial T$) for the
858 contemporary c_a and climate, using equations (A1) – (A3) above. (2) Use the e and
859 $\partial e/\partial T$ to calculate $\partial D/\partial T$ given the palaeo c_a (measured in ice-core data) and
860 temperature (reconstructed from pollen data), via a series of analytical equations that
861 relate $\partial e/\partial T$ to $\partial D/\partial T$ and hence to s . (3) Use the new $\partial D/\partial T$ and relative humidity (from
862 the PMIP3 average) to derive a new value of s . (4) Re-calculate MI using a palaeo
863 estimate of R_n (modelled as in Davis *et al.*, 2017) and the new value of s .